Published in final edited form as:

Adv Healthc Mater. 2021 August ; 10(15): e2002031. doi:10.1002/adhm.202002031.

Radiolabeling of Gold Nanocages for Potential Applications in Tracking, Diagnosis, and Image-Guided Therapy

Jichuan Qiu,

The Wallace H. Coulter Department of Biomedical Engineering, Georgia Institute of Technology and Emory University, Atlanta, Georgia 30332, USA

Yongjian Liu,

Department of Radiology, Washington University School of Medicine, St. Louis, Missouri 63110, USA

Younan Xia

The Wallace H. Coulter Department of Biomedical Engineering, Georgia Institute of Technology and Emory University, Atlanta, Georgia 30332, USA

School of Chemistry and Biochemistry, School of Chemical and Biomolecular Engineering, Georgia Institute of Technology, Atlanta, Georgia 30332, USA

Abstract

Gold nanocages (AuNCs) have emerged as a novel class of multifunctional nanomaterials with an array of applications in nanomedicine, including drug delivery, controlled release, as well as disease diagnosis and treatment. Labeling AuNCs with radionuclides not only offers additional therapeutic capabilities but also makes it easy to analyze their biodistribution, monitor their uptake by the tissue or organ of interest, and optimize their performance in both diagnosis and treatment. In this Progress Report, we begin with an introduction to the chemical synthesis and optical properties of AuNC. We then showcase several methods developed for their radiolabeling and highlight the use of radiolabeled AuNCs in tracking and quantifying their pharmacokinetics, including biodistribution, tumor uptake, and intratumoral distribution. Finally, we discuss their potential applications in targeted imaging and image-guided therapy.

Graphical Abstract

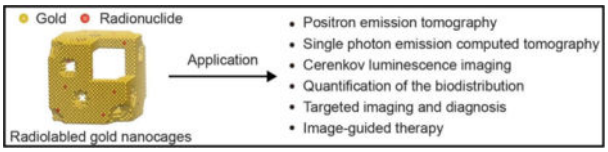

Labeling AuNCs with radionuclides makes them visible by positron emission tomography, single photon emission computed tomography, and Cerenkov luminescence imaging, offering the

younan.xia@bme.gatech.edu .

Conflict of Interest

The authors declare no conflict of interest.

convenience for analyzing their biodistribution, monitoring their uptake by the tissue or organ of interest, and optimizing their performance in image-guided therapy.

Keywords

gold nanocage; radiolabeling; molecular imaging; Cerenkov luminescence; image-guided therapy

1. Introduction

As a class of hollow nanocrystals, Au nanocages (AuNCs) feature ultrathin and porous walls comprised of Au or Au-based alloys. Owing to their unique properties, AuNCs have been actively explored for a variety of applications in biomedicine, including drug delivery, cancer diagnosis and treatment.[1–5] Specifically, their hollow structure provides a high capacity for loading various types of payloads, while the payload can be quickly loaded and released through the pores in the walls. These features are particularly attractive in drug delivery and controlled release.[5–7] In addition, the localized surface plasmon resonance (LSPR) peaks of AuNCs can be readily tuned to the near-infrared (NIR) region, allowing us to take advantage of the transparent window of soft tissues, where light can penetrate deeply with minimal attenuation. This feature makes AuNCs ideal candidates for *in vivo* optical imaging and therapeutic applications.[8] Furthermore, AuNCs exhibit a high efficiency for light-to-heat conversion under NIR irradiation, making them useful in photothermal therapy and/or thermo-responsive drug release.[9] Their sizes can also be tightly controlled in the range of 20–500 nm, allowing for optimization of their *in vivo* biodistribution profiles. Their surface can be conveniently conjugated with functional molecules through the gold–thiolate chemistry to achieve favorable interactions with the biological system of interest.[10] The last but not least, the good mechanical flexibility and stability associated with their single-crystal structure make it feasible for them to survive the complex *in vivo* environments.[2]

Among the various features of AuNCs, the capability for imaging is of great importance as it allows one to analyze their *in vivo* biodistribution, monitor their uptake by the tissue or organ of interest, and optimize their performance in both diagnosis and treatment.[11,12] Even though AuNCs themselves can serve as optical probes for two and three-photon luminescence imaging or as contrast agents for optical coherence tomography (OCT) and photoacoustic (PA) imaging, these modalities tend to be limited by intrinsic drawbacks such as limited penetration depth and low sensitivity.[12–16] In addressing these issues, we have labeled AuNCs with radionuclides to make them well-suited as contrast agents for molecular imaging, including positron emission tomography (PET) and single photon emission computed tomography (SPECT).[17,18] These imaging modalities exhibit unlimited penetration depth and ultra-high sensitivity *in vivo*, while only a trace amount of the contrast agent needs to be used.[19–21] They also provide other advantages, such as non-invasiveness, high patient compliance, and real-time quantification of the radioactive tracer concentration at target locations.[21–23] In addition, the decay of a radionuclide can generate Cerenkov luminescence, making it possible to combine nuclear imaging with optical imaging.[24,25] Different from conventional luminescence, Cerenkov luminescence does not need excitation light, making it possible for deep tissue imaging while eliminating the interference from

background autofluorescence.[25] More importantly, PET, SPECT, and radioluminescence imaging systems can be integrated together or with other anatomy-based imaging modalities such as computerized tomography (CT), leading to more precise detection and analysis.[21]

Herein, we summarize the recent developments in labeling AuNCs with radionuclides and their uses as contrast or imaging agents. We begin with a brief introduction to the chemical synthesis of AuNCs, as well as their basic properties. We then discuss the methods that have been developed for labeling AuNCs with radionuclides such as ^{198}Au, ^{199}Au, ^{64}Cu, and $^{64}Cu^{2+}$. Afterwards, we showcase the use of radiolabeled AuNCs for tracking and quantifying their biodistribution, tumor uptake, and intratumoral distribution. At the end, we offer a perspective on the potential use of radiolabeled AuNCs in targeted imaging and image-guided therapy.

2. Synthesis of AuNCs and Their Unique Properties

One can prepare AuNCs by taking advantage of the galvanic replacement reaction between Ag nanocubes and $HAuCl_4$, which can be described using the following equation:[26,27]

$$3Ag_{(s)} + \quad AuCl_4^-{}_{(aq)} \rightarrow Au_{(s)} + 3Ag^+_{(aq)} + 4Cl^-_{(aq)}$$

Since $AuCl_4^-$/Au (1.00 V) has a more positive standard reduction potential relative to Ag^+/Ag (0.80 V), Ag atoms can be directly oxidized into Ag^+ ions while the $AuCl_4^-$ will be reduced to Au atoms and deposited on the surface of the Ag nanocubes, leading to the formation of AuNCs. In practice, AuNCs with tunable LSPR peaks are typically produced by introducing aqueous $HAuCl_4$ into an aqueous suspension of Ag nanocubes with a syringe pump.[26] Figure 1, A and B, shows transmission electron microscopy (TEM) images of Ag nanocubes and the as-obtained AuNCs, respectively.[28] The nanocages had an average edge length of 45 nm, with a hollow interior and multiple pores (2–6 nm in diameter) in the wall. The morphological and structural evolutions from a Ag nanocube to a AuNC during the galvanic reaction is shown in Figure 1C. Detailed discussions can be found in other review articles.[1,9] Both the size and shape of the AuNCs can be easily tuned by varying the Ag nanocrystal template. In addition to Ag, Cu nanocrystals could serve as a sacrificial template for the fabrication of Au-based nanocages.[29] It is worth mentioning that AuNCs have also been synthesized *via* seed-mediated growth of Au on a template (*e.g.,* Ag or Pd nanocrystal), followed by selective removal of the template from the core through chemical etching. Using this method, the wall thickness of the final AuNCs can be reduced down to several layers of Au atoms by controlling the seed-mediated deposition process.[30]

One of the most appealing properties of AuNCs is their tunable LSPR peaks in visible and NIR regions. LSPR refers to the scattering and absorption of incident light at a specific wavelength due to the collective oscillation of conduction electrons in the metal nanostructure at the same resonant frequency.[31–33] The LSPR peak of the AuNCs can be tuned by varying their size, composition, as well as the wall thickness and porosity. Figure 1D shows UV–vis–NIR extinction spectra of aqueous suspensions of AuNCs prepared by reacting a fixed amount of Ag nanocubes with different amounts of $HAuCl_4$ solutions,

showing that the optical properties of AuNCs are strongly correlated with the degree of galvanic replacement reaction (*i.e.*, the composition and porosity of the final products).[26] Accordingly, the color of the samples changes from yellow to reddish-brown, purple, and blue (Figure 1E). Due to the LSPR effect, AuNCs are able to scatter and absorb light very strongly, making them useful as contrast agents for optical imaging or as photothermal agents for a variety of niche applications.[9] These capabilities are particularly relevant to biomedical applications considering that the LSPR peak of AuNCs can be precisely tuned into the transparent window of soft tissues. In addition, AuNCs also holds great promises for translational application considering their good biocompatibility both *in vitro* and *in vivo*.[34]

3. Substitution of Au Atoms with ^{198}Au or ^{199}Au Atoms

The simplest and most straightforward method for labeling AuNCs with a radionuclide is to partially substitute the Au atoms in the walls with one of its radioactive isotopes, such as ^{198}Au (β^-=0.96 MeV, $t_{1/2}$= 2.7 days) or ^{199}Au (β^-=0.452 MeV, $t_{1/2}$= 3.1 days). The substitution can be readily realized by employing a mixture of $H^{198}AuCl_4$ (or $H^{199}AuCl_4$) and $HAuCl_4$ as the precursor to Au atoms.[35] Figure 2A shows the preparation of ^{198}Au-doped AuNCs through the galvanic replacement reaction between Ag nanocubes and a mixture of $H^{198}AuCl_4$ and $HAuCl_4$. The mixture of $H^{198}AuCl_4$ and $HAuCl_4$ was formed by irradiating a piece of nonradioactive Au foil with neutrons, followed by dissolution of the foil in aqua regia. Further purification was achieved by heating the products at 130 °C to remove the acids and other byproducts such as NO_2 and NO.[36,37] Figure 2B shows a TEM image of the ^{198}Au-doped AuNCs (after the complete decay of ^{198}Au), with an average edge length of 33 nm. They exhibited the same shape and structure as the samples prepared with $HAuCl_4$ alone. The radioactive thin layer chromatography in Figure 2C confirmed the radioactivity of the as-obtained AuNCs. Since there was no detection of unbound $^{198}Au^{3+}$, the ^{198}Au atoms were stably incorporated into the walls of the nanocages. As expected, the specific radioactivity of the final AuNCs could be tuned by varying the concentration of $H^{198}AuCl_4$ in the precursor mixture.

The energy of β^- emitted from ^{198}Au significantly exceeds 0.26 MeV, the threshold of kinetic energy required for Cerenkov radiation in biological tissues.[24] As a result, ^{198}Au-doped AuNCs are able to emit a high throughput of Cerenkov luminescence with wavelengths in the visible and NIR regions.[35] This feature enables the direct observation and tracking of the spatial distribution of the AuNCs injected into a mouse. Figure 2D shows the luminescent images of a mouse bearing an EMT-6 tumor after intravenous injection of ^{198}Au-doped AuNCs (2.37 MBq. per mouse) for 0, 2, and 24 h, respectively. To improve the circulation time in the bloodstream and the accumulation in the tumor, the surface of the AuNCs were conjugated with poly(ethylene glycol) (PEG) prior to the injection.[38–40] Clearly, the luminescence rapidly increased at the tumor, spleen, and liver sites in the first 24 h after injection, indicating the accumulation of AuNCs in these tissues or organs. As a major advantage of this method, ^{198}Au atoms are directly incorporated into the solid lattice of AuNCs, ensuring the stability for *in vivo* imaging and accurate analysis. Similarly, ^{199}Au atoms can also be incorporated into the walls of AuNCs by mixing $H^{199}AuCl_4$, instead of

$H^{198}AuCl_4$, with the $HAuCl_4$ precursor.[41] In general, the scope of this method is only limited by the availability of radioactive isotopes of Au.

4. Conjugation of $^{64}Cu^{2+}$ Cations through Chelating Ligands

Because of its desirable nuclear properties ($t_{1/2}$ = 12.7 h, β^+ = 17%, and β^- = 40%), ^{64}Cu has become one of the most commonly used radionuclides in nanomedicine.[22] It can be readily introduced into the surface of a nanoparticle in the ionic form through the use of a specific chelating ligand.[42,43] In one demonstration, $^{64}Cu^{2+}$ ions were conjugated to the surface of AuNCs with the aid of 1,4,7,10-tetraazacyclododacane-1,4,7,10-tetraacetic acid (DOTA), a macrocyclic chelating ligand.[17] The major steps involved in this conjugation are summarized in Figure 3A. In the first step, hetero-functional PEG was modified to the surface of AuNCs through the Au–S reaction to generate PEGylated AuNCs with NH_2 groups on their surface. The NH_2 groups were then coupled to 1,4,7,10-tetraazacyclododacane-1,4,7,10-tetraacetic acid mono(N-hydroxysuccinimide ester) (DOTA-NHS-ester) through the amide reaction *via* NHS-activated ester. Upon incubation with $^{64}Cu^{2+}$ ions, $^{64}Cu^{2+}$-labeled AuNCs (denoted ^{64}Cu-DOTA-PEG-AuNCs) could be obtained by removing the free $^{64}Cu^{2+}$ through centrifugation. The as-labeled AuNCs were able to retain >80% of the radioactivity after incubation in 10% mouse serum (in PBS) for 24 h, demonstrating the good stability.

These $^{64}Cu^{2+}$-labeled AuNCs also exhibited high specific radioactivity and stability *in vivo*. Figure 3B shows PET/CT images of a mouse bearing an EMT-6 tumor after tail vein injection of a trace amount (23.8 fmol for AuNCs or 3.7 MBq for radioactivity) of ^{64}Cu-DOTA-PEG-AuNCs with an edge length of 30 nm for 1, 4, and 24 h, respectively. The $^{64}Cu^{2+}$-labeled AuNCs were initially detected at the center of the tumor and they rapidly spread throughout the tumor within 24 h. A quantitative analysis of the PET images further confirmed that the ratio of the nanocages accumulated in tumor relative to those in muscle kept increasing in the first 24 h. As a major advantage, this approach is extendible to other types of radioactive metal ions as long as appropriate chelating ligands can be identified. However, it is worth pointing out that the residual Ag in the AuNCs should be removed before labeling with $^{64}Cu^{2+}$ ions. Otherwise, the Ag^+ ions leaked from the walls would compete for the DOTA chelator, significantly decreasing the number of DOTA chelators available for $^{64}Cu^{2+}$ radiolabeling.[44] Moreover, the surface characteristics of AuNCs may be altered by the macrocyclic ligands, leading to a reduced loading capability for other types of ligands (*e.g.*, targeting or therapeutic molecules). Another potential issue is that the chelated $^{64}Cu^{2+}$ ions may be trans-chelated to proteins *in vivo*, resulting in high uptake by off-target tissues or organs and thus misinterpretation of the imaging data.[35]

5. Alloying with ^{64}Cu Atoms

It is also feasible to have ^{64}Cu atoms directly deposited on the surface of Au nanoparticles to achieve radiolabeling.[45–47] A recent study demonstrated this approach for AuNCs through the co-reduction of $HAuCl_4$, $CuCl_2$, and $^{64}CuCl_2$ in the presence of pre-formed AuNCs.[18] Figure 4A shows the schematic illustration of such a synthesis. During deposition, the Au, Cu, and ^{64}Cu atoms formed an alloy on the surface of the AuNCs. The TEM image in Figure

4B demonstrates that the resultant AuNCs preserved the unique features of the original nanocages, including the hollow structure and the pores at the corner sites. The ^{64}Cu-labeled nanocages had an edge length of 44 nm, together with a Au-Cu alloy shell of 3.6 nm in thickness. The thickness of the alloy layer could be adjusted by introducing different amounts of metal precursors into the reaction system while the radioactivity of the resultant AuNCs could be tuned by varying the proportion of $^{64}CuCl_2$ in the precursor mixture.[31]

When 7.4 MBq of $^{64}CuCl_2$ was used for the co-deposition process, the specific radioactivity of the ^{64}Cu-doped AuNCs reached 2.04 GBq/nmol. Importantly, this strategy demonstrated superior radiolabeling stability for accurate tracking AuNCs *in vivo*.[18,46] Figure 4C shows PET/CT images of mice 4T1 and patient-derived xenografts (PDX) tumor models after tail vein injection of the ^{64}Cu-doped AuNCs for 24 h, indicating the accumulation of the nanocages in the tumors for both animal models. The autoradiography of tumor tissues further demonstrates the homogeneous intratumoral distribution of the nanocages. Quantification of the uptake in these two tumor models also confirmed their gradual accumulation (Figure 4D). For the ^{64}Cu and Cu atoms that were directly deposited on the surface of AuNCs in the form of an alloy with Au atom, their stability should be much greater than the $^{64}Cu^{2+}$ ions that are conjugated to the surface through chelating ligands. It is worth mentioning that the deposition of Cu-Au alloy on the surface of AuNCs will induce a blue shift to their LSPR peak, which needs to be taken into consideration in choosing the pre-formed AuNCs.[18]

6. Quantifying the Biodistribution and Intratumoral Accumulation

It has been demonstrated that the intravenously-injected AuNCs typically circulate in the bloodstream and accumulate in tumor and organs such as liver, spleen, lung, and kidney.[17,48] It is still not clear how AuNCs will be cleaned from the body. Their relatively large size makes it difficult for them to undergo renal clearance, while the extraordinary chemical stability of Au also make it difficult to have AuNCs metabolized in vivo. Due to the bioinertness of Au, the AuNCs should be able to remain in the body without eliciting adverse impacts. To this end, it is of critical importance to quantify the pharmacokinetics of AuNCs, including their biodistribution, tumor uptake, and intratumoral accumulation. As mentioned above, labeling AuNCs with radionuclides offers an opportunity for direct observation, tracking, and analysis of their distribution *in vivo* by PET, SPECT, or radioluminescence imaging.[1,17,35] By comparing the intensities of signals originating from different tissues or organs, one can semi-quantitively analyze the overall distribution of AuNCs. Their accumulation in solid tumors or other specific organs could be derived from the changes in intensity over time. For example, after labeling 33-nm AuNCs with ^{198}Au, one can directly observe their accumulation in the tumor, as well as spleen and liver in the first 24 h after injection under an optical imaging system by leveraging the Cerenkov luminescence of ^{198}Au (see Figure 2D).[35]

The biodistribution of AuNCs could also be quantified by tracing the γ radiation from the radionuclide in each organ *ex vivo*.[17,49] In one demonstration, the *in vivo* distribution of the four types of Au nanostructures, including nanospheres, nanodisks, nanorods, and nanocages, were systematically investigated by incorporating ^{198}Au into their solid lattice.

[49] Specifically, these Au nanostructures were prepared using a mixture of $H^{198}AuCl_4$ and $HAuCl_4$ as the precursor. Figure 5, A–D, shows TEM images of the four samples. After modification with PEG, the four types of radiolabeled Au nanostructures were injected into tumor-bearing mice through tail vein, respectively. The organs of interest were collected at different time points post injection for gamma counting. Figure 5, E and F, hows a comparison of the biodistributions of these four types of ^{198}Au-labeled Au nanostructures at 1 and 24 h post injection, respectively. Clearly, all four samples showed high accumulation in liver and spleen. However, for these four types of Au nanostructures with different shapes, their *in vivo* pharmacokinetic profiles were significantly different. For example, the Au nanospheres showed a much longer circulation in bloodstream than the other three types of nanostructures, with a percent injected dose per gram of tissue (% ID/g) of 24.8% at 6 h. The AuNCs showed the second-longest blood circulation, which was maintained at a level of 14.2% ID/g at 6 h post injection. As for the accumulation in tumors, Au nanospheres showed the greatest level, with up to 23.2% ID/g at 24 h post injection, while AuNCs gave about 7.5% ID/g.

In addition to quantifying the biodistributions of these Au nanostructures, the radiolabeling also allowed us to monitor and analyze their intratumoral distributions.[17] Typically, after injection of the labeled nanostructures into tumor-bearing mice for 24 h, the tumors were excised and then microtomed into slices of 50 μm in thickness. These slices were then characterized by the autoradiography imaging. Figure 6 shows the as-obtained autoradiographic images of the tumor slices involving the four different types of ^{198}Au-doped Au nanostructures.[49] Specifically, the nanospheres and nanodisks were mainly concentrated in the periphery of the tumors, while the nanorods and nanocages appeared throughout the tumor, with the strongest signal coming from the core of the tumor. It has been established that nanoparticles enter tumors by leaking out through the intracellular gaps of the chaotic and hyperpermeable vasculature of a tumor based on the enhanced permeability and retention (EPR) effect.[50,51] The size, shape, and surface properties of the nanostructures influence not only their accumulation in a tumor but also the intratumoral distribution. For tumor therapy, nanostructures capable of quickly populating the entire tumor volume will give a better performance for the complete removal of the lesions, avoiding cancer relapse or metastasis.[52,53] Considering the overall performance in terms of blood circulation, tumor accumulation, and intratumoral distribution, AuNCs should be more attractive in cancer therapy compared to other types of nanostructures. More importantly, the hollow interior of AuNCs provides a high loading capacity for drugs, making them more viable in drug delivery-based cancer therapy.

7. Targeted Imaging and Diagnosis

Upon radiolabeling, AuNCs can serve as contrast agents not only for the evaluation of their biodistribution *in vivo* but also for targeted imaging of cells or tissues. For example, selective delivery of the radiolabeled AuNCs into a solid tumor can be used for cancer diagnosis. Despite some progress, it remains a grand challenge to effectively deliver nanoparticles into the tumor by leveraging the EPR effect only.[49,54] An alternative strategy is to functionalize their surfaces with a ligand that can selectively bind to a receptor (*i.e.*, biomarker) overexpressed on the surface of the cancer cells.[55–57] In one demonstration,

[Nle^4, D-Phe^7]-α-melanocyte-stimulating hormone (NDP-α-MSH), a peptide capable of strongly binding to the α-MSH receptor overexpressed on melanoma cells, were conjugated to the surface of AuNCs, together with $^{64}Cu^{2+}$ ions for targeted imaging of melanoma.[58] In a typical process, NDP-α-MSH and DOTA were linked to PEG chains terminated with orthopyridyl disulfide groups, respectively, followed by conjugation to AuNCs with an edge length of 35 nm through the Au–S linkage. By chelation with DOTA, $^{64}Cu^{2+}$ ions could then be introduced onto the surface of the AuNCs, generating both NDP-α-MSH- and $^{64}Cu^{2+}$-labeled AuNCs (denoted ^{64}Cu-AuNC-PEG-MSH). After injection into mice bearing B16/F10 melanoma, ^{64}Cu-AuNC-PEG-MSH showed higher accumulation in the melanoma model at 24 h post injection when compared to AuNCs without labeling with NDP-α-MSH, demonstrating the targeting ability of ^{64}Cu-AuNC-PEG-MSH. In principle, the targeting efficiency of ^{64}Cu-AuNCs-PEG-MSH could be further increased by optimizing the number of NDP-α-MSH peptides present on the surface of each AuNC.[58]

8. Perspective: Potential Use in Image-Guided Therapy

Due to the extraordinary efficiency in photo-to-heat conversion, AuNCs have been used as photothermal agents for the ablation of solid tumors.[59,60] After accumulation in a solid tumor, the nanocages are able to quickly elevate the temperature within the tumorous tissues under the irradiation of light, causing damage to the lesion tissue by destroying the normal structure and function of proteins. In the meantime, the well-defined hollow and porous structures of AuNCs can be used as effective drug carriers while the loaded drugs will be released in response to light irradiation by leveraging the photothermal effect.[61–64] Significantly, the LSPR peaks of the AuNCs can be tuned into the NIR window of soft tissues, making it possible for the treatment of deep malignancy below the skin.[9]

When labeled with a radionuclide, AuNCs can serve as a multifunctional platform for image-guided therapy to precisely quantify the AuNCs delivered into a tumor for optimizing treatment regimen and thus improving the outcome.[65–67] Figure 7A shows a schematic to illustrate how the radiolabeled AuNCs can be applied to image-guided cancer therapy. After injection, the AuNCs will be delivered to the tumor site through passive and/or active targeting. Benefiting from the ultra-high sensitivity and deep penetration of molecular imaging (*e.g.*, PET) or radioluminescence imaging modalities, one can confirm the precise margins or boundaries of the lesion tissues. At the same time, the biodistribution and intratumoral accumulation of the AuNCs can be monitored and quantified using the same imaging system. Based on the imaging results, the NIR laser will be applied to the exact site with appropriate duration and powder to ensure that the cancer cells are eradicated efficiently while the surrounding healthy tissues are kept safe. Under NIR irradiation, the AuNCs are able to eradicate cancer cells through photothermal heating (Figure 7B) and/or photothermally-triggered drug release (Figure 7C). To enable controlled release, the drugs can be co-loaded into the nanocages with a thermo-responsive matrix such as a phase-change material (PCM).[60–62] Upon heating under NIR irradiation, the PCM will be melted to trigger the release of drugs for more effectively killing the cancer cells.[68,69]

In conclusion, we have introduced several strategies for the radiolabeling of AuNCs, together with their applications in serving as probes for molecular imaging and

radioluminescence imaging. The Au isotypes (*e.g.*, ^{198}Au or ^{199}Au) can be directly incorporated into the walls of AuNCs in the form of atoms during the synthesis involving galvanic replacement reaction. Other radionuclides (*e.g.,* ^{64}Cu) can be added to the surface of AuNCs through either conjugation with the aid of a chelating agent or co-deposition with Au atoms. After radiolabeling, the pharmacokinetics of the AuNCs including the biodistribution, tumor uptake, and intratumoral accumulation can be easily observed and quantified by leveraging the radioactivity and Cerenkov luminescence. These radiolabeled AuNCs hold great promises for disease diagnosis upon additional modification with targeting ligands, as well as image-guided therapy by leveraging their photothermal properties and drug delivery capability. As a major difference from the conventional materials, researchers need to pay close attention to the lab safety when working with radiolabeled AuNCs, in addition to their *in vivo* stability and biosafety.

Acknowledgments

This work was supported in part by startup funds from the Georgia Institute of Technology, a grant from the National Institutes of Health (NIH, R01 CA138527), and an NIH Director's Pioneer Award (DP1 OD000798). We are grateful to our coworkers and collaborators for their invaluable contributions to this project.

References

[1]. Xia Y, Li W, Cobley CM, Chen J, Xia X, Zhang Q, Yang M, Cho EC, Brown PK, Acc. Chem. Res 2011, 44, 914. [PubMed: 21528889]

[2]. Yang X, Yang M, Pang B, Vara M, Xia Y, Chem. Rev 2015, 115, 10410. [PubMed: 26293344]

[3]. Chen J, Yang M, Zhang Q, Cho EC, Cobley CM, Kim C, Glaus C, Wang LV, Welch MJ, Xia Y, Adv. Funct. Mater 2010, 20, 3684. [PubMed: 33907543]

[4]. Skrabalak SE, Chen J, Au L, Lu X, Li X, Xia Y, Adv. Funct. Mater 2007, 19, 3177.

[5]. Skrabalak SE, Chen J, Sun Y, Lu X, Au L, Cobley CM, Xia Y, Acc. Chem. Res, 2008, 41, 1587. [PubMed: 18570442]

[6]. Qiu J, Xu J, Xia Y, Adv. Healthcare Mater 2020, 2000587.

[7]. Yang M, Wang W, Qiu J, Bai M-Y, Xia Y, Angew. Chem. Int. Ed 2019, 58, 17671.

[8]. Dreaden EC, Alkilany AM, Huang X, Murphy CJ, El-Sayed MA, Chem. Soc. Rev 2012, 41, 2740. [PubMed: 22109657]

[9]. Qiu J, Xie M, Wu T, Qin D, Xia Y, Chem. Sci 2020, 11, 12955.

[10]. Chen J, Saeki F, Wiley BJ, Cang H, Cobb MJ, Li Z-Y, Au L, Zhang H, Kimmey MB, Li X, Xia Y, Nano Lett. 2005, 5, 473. [PubMed: 15755097]

[11]. Song KH, Kim C, Cobley CM, Xia Y, Wang LV, Nano Lett. 2009, 9, 183. [PubMed: 19072058]

[12]. Kim C, Cho EC, Chen J, Song KH, Au L, Favazza C, Zhang Q, Cobley CM, Gao F, Xia Y, Wang LV, ACS Nano 2010, 4, 4559. [PubMed: 20731439]

[13]. Yang X, Skrabalak SE, Li Z-Y, Xia Y, Wang LV, Nano Lett. 2007, 7, 3798. [PubMed: 18020475]

[14]. Tong L, Cobley CM, Chen J, Xia Y, Cheng J-X, Angew. Chem. Int. Ed 2010, 49, 3485.

[15]. Huang X, Neretina S, El-Sayed MA, Adv. Mater 2009, 21, 4880. [PubMed: 25378252]

[16]. Gao L, Fei J, Zhao J, Li H, Cui Y, Li J, ACS Nano 2012, 6, 8030. [PubMed: 22931130]

[17]. Wang Y, Liu Y, Luehmann H, Xia X, Brown P, Jarreau C, Welch M, Xia Y, ACS Nano 2012, 6, 5880. [PubMed: 22690722]

[18]. Yang M, Huo D, Gilroy KD, Sun X, Sultan D, Luehmann H, Detering L, Li S, Qin D, Liu Y, Xia Y, ChemNanoMat 2017, 3, 44.

[19]. Ametamey SM, Honer M, Schubiger PA, Chem. Rev 2008, 108, 1501. [PubMed: 18426240]

[20]. Blodgett TM, Meltzer CC, Townsend DW, Radiology 2007, 242, 360. [PubMed: 17255408]

[21]. Ge J, Zhang Q, Zeng J, Gu Z, Gao M, Biomaterials 2020, 228, 119553. [PubMed: 31689672]

[22]. Liu Y, Welch MJ, Bioconjug. Chem 2012, 23, 671. [PubMed: 22242601]
[23]. Guo Y, Aweda T, Black KCL, Liu Y, Curr. Top. Med. Chem 2013, 13, 470. [PubMed: 23432009]
[24]. Xu Y, Liu H, Cheng Z, J. Nucl. Med 2011, 52, 2009. [PubMed: 22080446]
[25]. Lucignani G, Eur. J. Nucl. Med. Mol. Imaging 2011, 38, 592. [PubMed: 21174087]
[26]. Skrabalak SE, Au L, Li X, Xia Y, Nat. Protoc 2007, 2, 2182. [PubMed: 17853874]
[27]. Sun Y, Mayers BT, Xia Y, Nano Lett. 2002, 2, 481.
[28]. Xia X, Xia Y, Front. Phys 2014, 9, 378.
[29]. Xie S, Jin M, Tao J, Wang Y, Xie Z, Zhu Y, Xia Y, Chem. Eur. J 2012, 18, 14974. [PubMed: 23108763]
[30]. Sun X, Kim J, Gilroy KD, Liu J, König TAF, Qin D, ACS Nano 2016, 10, 8019. [PubMed: 27458731]
[31]. Cobley CM, Chen J, Cho EC, Wang LV, Xia Y, Chem. Soc. Rev 2011, 40, 44. [PubMed: 20818451]
[32]. Kreibig U, Vollmer M, Optical Properties of Metal Clusters, Springer Science & Business Media, 2013.
[33]. Hutter E, Fendler JH, Adv. Mater 2004, 16, 1685.
[34]. Wang Y, Black KCL, Luehmann H, Li W, Zhang Y, Cai X, Wan D, Liu S-Y, Li M, Kim P, Li Z-Y, Wang LV, Liu Y, Xia Y, ACS Nano 2013, 7, 2068. [PubMed: 23383982]
[35]. Wang Y, Liu Y, Luehmann H, Xia X, Wan D, Cutler C, Xia Y, Nano Lett. 2013, 13, 581. [PubMed: 23360442]
[36]. Zhou C, Hao G, Thomas P, Liu J, Yu M, Sun S, Öz OK, Sun X, Zheng J, Angew. Chem. Int. Ed 2012, 51, 10118.
[37]. Herrmann WA, Synthetic Methods of Organometallic and Inorganic Chemistry: Copper, Silver, Gold, Zinc, Cadmium and Mercury, Thieme: New York, 1999.
[38]. Sun T, Zhang YS, Pang B, Hyun DC, Yang M, Xia Y, Angew. Chem. Int. Ed 2014, 53, 12320.
[39]. Yang X, Yang M, Pang B, Vara M, Xia Y, Chem. Rev 2015, 115, 10410. [PubMed: 26293344]
[40]. Blanco E, Shen H, Ferrari M, Nat. Biotechnol 2015, 33, 941. [PubMed: 26348965]
[41]. Zhao Y, Pang B, Luehmann H, Detering L, Yang X, Sultan D, Harpstrite S, Sharma V, Cutler CS, Xia Y, Liu Y, Adv. Healthcare Mater 2016, 5, 928.
[42]. Wadas TJ, Wong EH, Weisman GR, Anderson CJ, Chem. Rev 2010, 110, 2858. [PubMed: 20415480]
[43]. Zeng D, Lee NS, Liu Y, Zhou D, Dence CS, Wooley KL, Katzenellenbogen JA, Welch MJ, ACS Nano 2012, 6, 5209. [PubMed: 22548282]
[44]. Kodama M, Mahatma AB, Koike T, Kimura E, Bull. Chem. Soc. Jpn 1990, 63, 2803.
[45]. Zhao Y, Sultan D, Detering L, Luehmann H, Liu Y, Nanoscale 2014, 6, 13501. [PubMed: 25266128]
[46]. Zhao Y, Sultan D, Detering L, Cho S, Sun G, Pierce R, Wooley KL, Liu Y, Angew. Chem. Int. Ed 2014, 126, 160.
[47]. Pang B, Zhao Y, Luehmann H, Yang X, Detering L, You M, Zhang C, Zhang L, Li Z-Y, Ren Q, Liu Y, Xia Y, ACS Nano 2016, 10, 3121. [PubMed: 26824412]
[48]. Poon W, Kingston BR, Ouyang B, Ngo W, Chan WCW, Nat. Nanotechnol 2020, 15, 819. [PubMed: 32895522]
[49]. Black KCL, Wang Y, Luehmann HP, Cai X, Xing W, Pang B, Zhao Y, Cutler CS, Wang LV, Liu Y, Xia Y, ACS Nano 2014, 8, 4385. [PubMed: 24766522]
[50]. Matsumura Y, Maeda H, Cancer Res. 1986, 46, 6387. [PubMed: 2946403]
[51]. Jain RK, Stylianopoulos T, Nat. Rev. Clin. Oncol 2010, 7, 653. [PubMed: 20838415]
[52]. Holback H, Yeo Y, Pharm. Res 2011, 28, 1819. [PubMed: 21213021]
[53]. Minchinton AI, Tannock IF, Nat. Rev. Cancer 2006, 6, 583. [PubMed: 16862189]
[54]. Rosenblum D, Joshi N, Tao W, Karp JM, Peer D, Nat. Commun 2018, 9, 1410. [PubMed: 29650952]

[55]. Sun T, Wang Y, Wang Y, Xu J, Zhao X, Vangveravong S, Mach RH, Xia Y, Adv. Healthcare Mater 2014, 3, 1283.

[56]. Khan SA, Kanchanapally R, Fan Z, Beqa L, Singh AK, Senapati D, Ray PC, Chem. Comm 2012, 48, 6711. [PubMed: 22627619]

[57]. Huang S, Duan S, Wang J, Bao S, Qiu X, Li C, Liu Y, Yan L, Zhang Z, Hu Y, Adv. Funct. Mater 2016, 26, 2532.

[58]. Zhao Y, Pang B, Detering L, Luehmann H, Yang M, Black K, Sultan D, Xia Y, Liu Y, Mol. Imaging 2018, 17, 1–9.

[59]. Chen J, Wang D, Xi J, Au L, Siekkinen A, Warsen A, Li Z-Y, Zhang H, Xia Y, Li X, Nano Lett. 2007, 7, 1318. [PubMed: 17430005]

[60]. Chen J, Glaus C, Laforest R, Zhang Q, Yang M, Gidding M, Welch MJ, Xia Y, Small 2010, 6, 811. [PubMed: 20225187]

[61]. Moon GD, Choi S-W, Cai X, Li W, Cho EC, Jeong U, Wang LV, Xia Y, J. Am. Chem. Soc 2011, 133, 4762. [PubMed: 21401092]

[62]. Chen Q, Huo D, Cheng H, Lyu Z, Zhu C, Guan B, Xia Y, Adv. Healthcare Mater 2019, 8, 1801113.

[63]. Cheng H, Huo D, Zhu C, Shen S, Wang W, Li H, Zhu Z, Xia Y, Biomaterials 2018, 178, 517. [PubMed: 29631784]

[64]. Yavuz MS, Cheng Y, Chen J, Cobley CM, Zhang Q, Rycenga M, Xie J, Kim C, Song KH, Schwartz AG, Wang LV, Xia Y, Nat. Mater 2009, 8, 935. [PubMed: 19881498]

[65]. Xu X, Chong Y, Liu X, Fu H, Yu C, Huang J, Zhang Z, Acta Biomater. 2019, 84, 328. [PubMed: 30500447]

[66]. Srivatsan A, Jenkins SV, Jeon M, Wu Z, Kim C, Chen J, Pandey RK, Theranostics 2014, 4, 163. [PubMed: 24465274]

[67]. Chen H, Zhang W, Zhu G, Xie J, Chen X, Nat. Rev. Mater 2017, 2, 17024. [PubMed: 29075517]

[68]. Qiu J, Huo D, Xia Y, Adv. Mater 2020, 32, 2000660.

[69]. Qiu J, Huo D, Xue J, Zhu G, Liu H, Xia Y, Angew. Chem. Int. Ed 2019, 58, 10606.

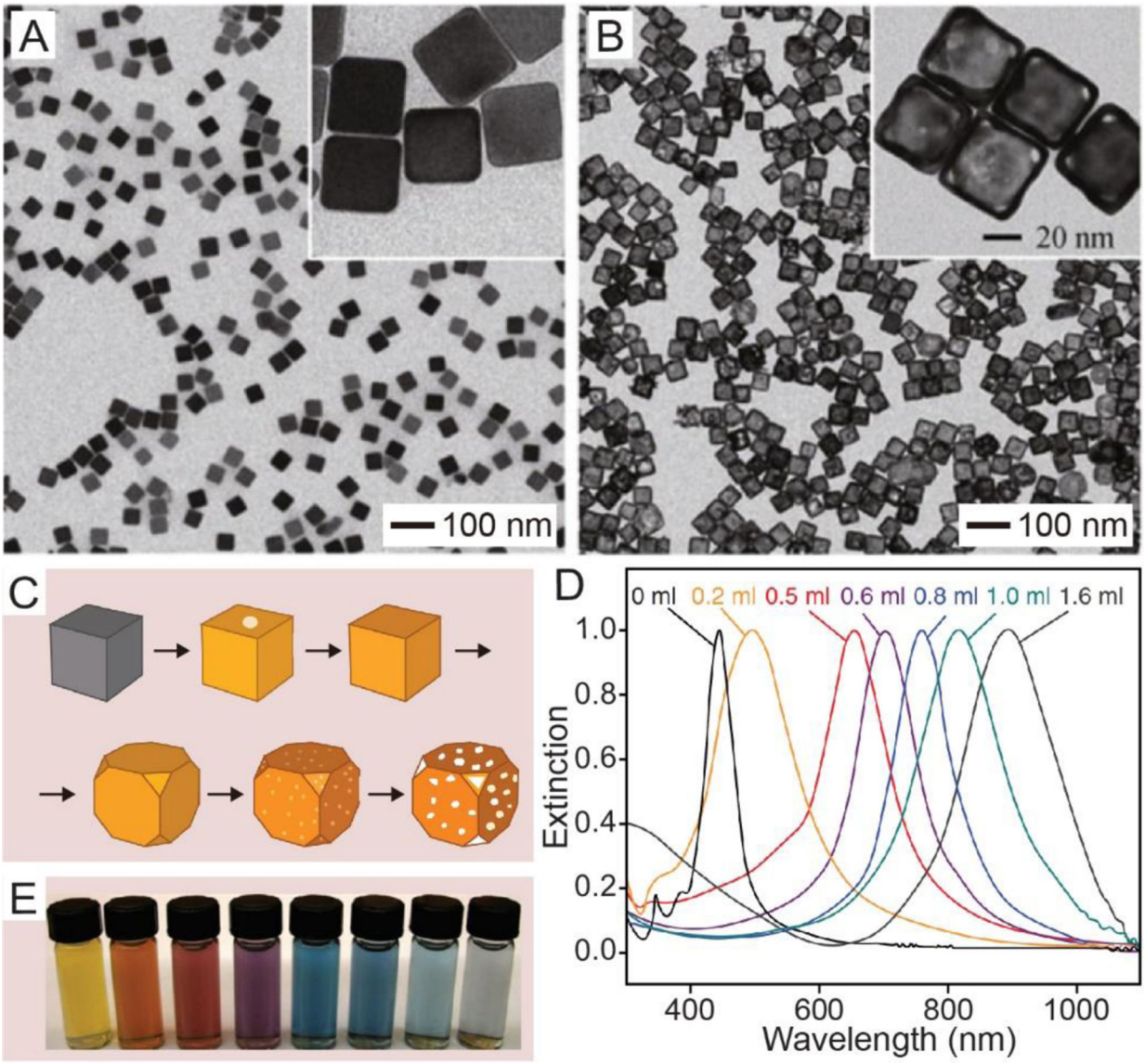

Figure 1.

TEM images of (A) Ag nanocubes and (B) AuNCs. (C) Schematic illustration of the structural changes during the synthesis of AuNCs from Ag nanocubes. (D) UV-vis spectra and (E) digital photographs of the suspension of Ag nanocubes upon reaction with different volumes of an aqueous $HAuCl_4$ solution. (A–C) Reproduced with permission.[28] Copyright 2014, Springer Nature. (D, E) Reproduced with permission.[26] Copyright 2007, Springer Nature.

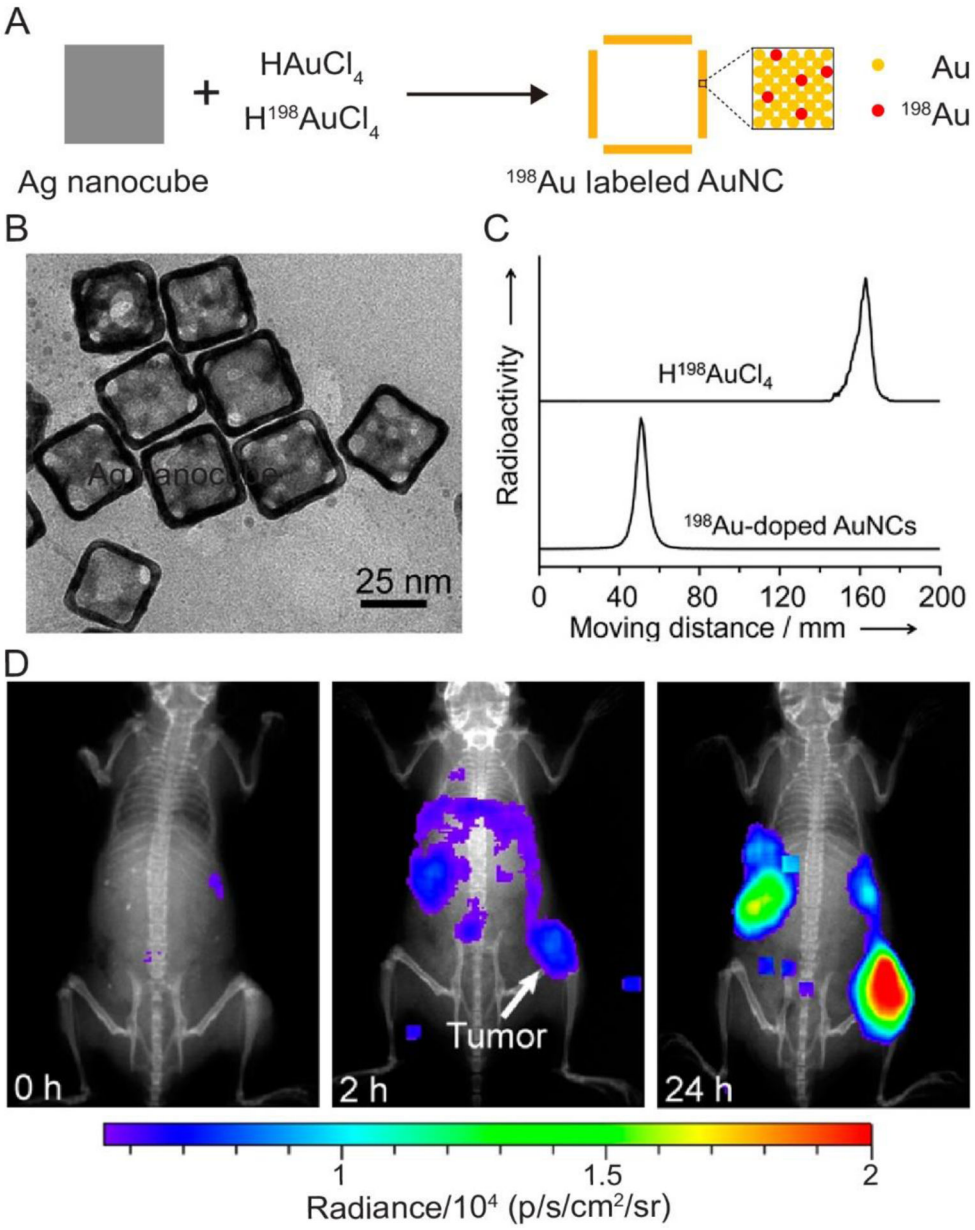

Figure 2.

(A) Schematic illustration showing the synthesis of radiolabeled AuNCs through the substitution of Au atoms with ^{198}Au atoms. (B) TEM image of the ^{198}Au-doped AuNCs, which was obtained after the ^{198}Au had decayed for one month. (C) Paper chromatography analyses of the $H^{198}AuCl_4$ and ^{198}Au-doped AuNCs. (D) Representative luminescence images of a mouse bearing an EMT-6 tumor after tail vein injection of the PEGylated, ^{198}Au-doped AuNCs (2.37 MBq per mouse) for 0, 2, and 24 h, respectively. The images were obtained by collecting the emission light in the range of 500–650 nm using a IVIS Lumina II XR System, with the excitation filter closed. Reproduced with permission.[35] Copyright 2013, American Chemical Society.

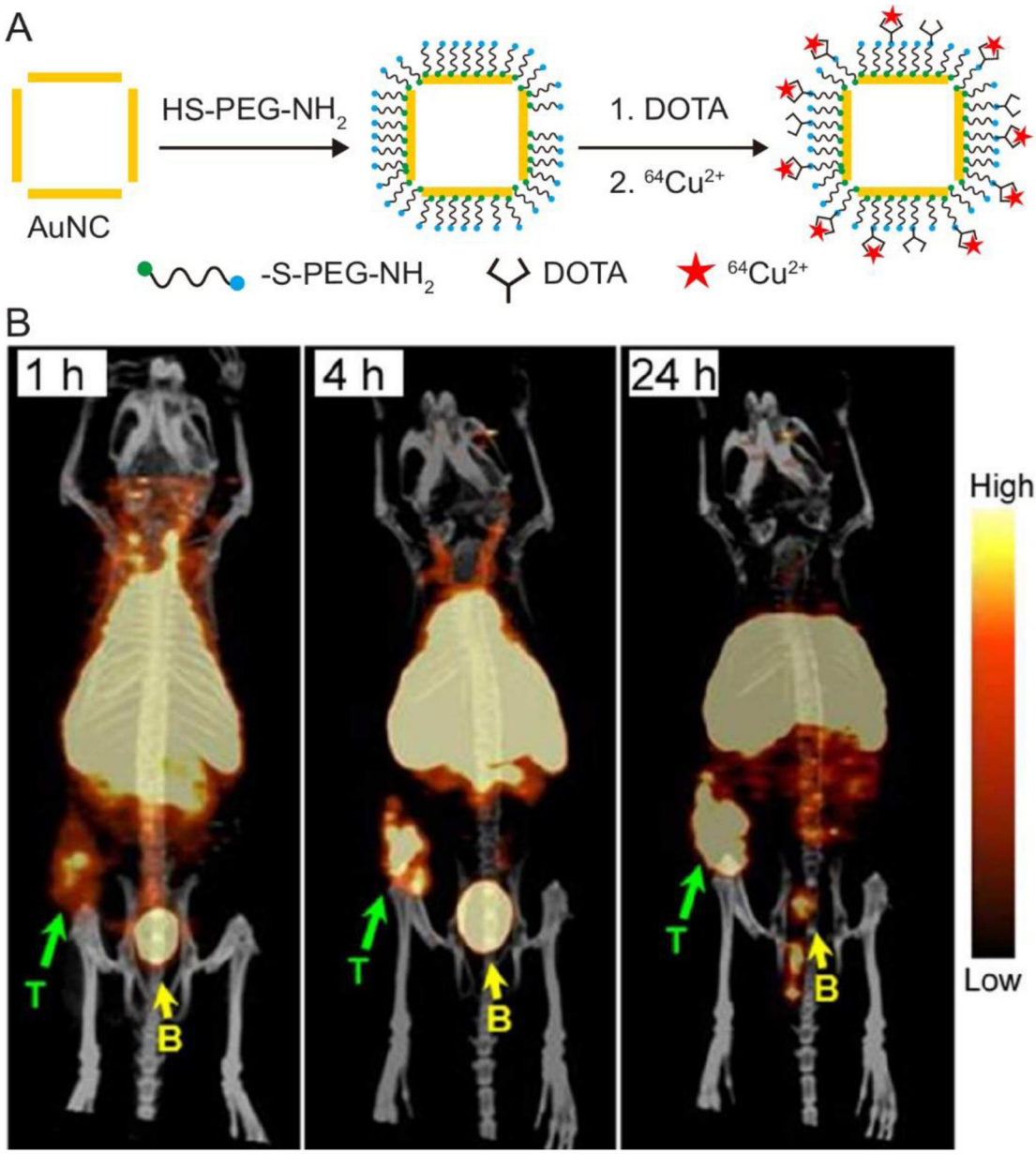

Figure 3.

Schematic illustration showing conjugation of $^{64}Cu^{2+}$ to the surface of a AuNC through DOTA, a chelating ligand. (B) PET/CT images of the 30-nm ^{64}Cu-DOTA-PEG-AuNCs in a mouse bearing an EMT-6 tumor at 1, 4, and 24 h post injection (3.7 MBq injection/mouse). T, tumor; B, ladder. Reproduced with permission.[17] Copyright 2012, American Chemical Society.

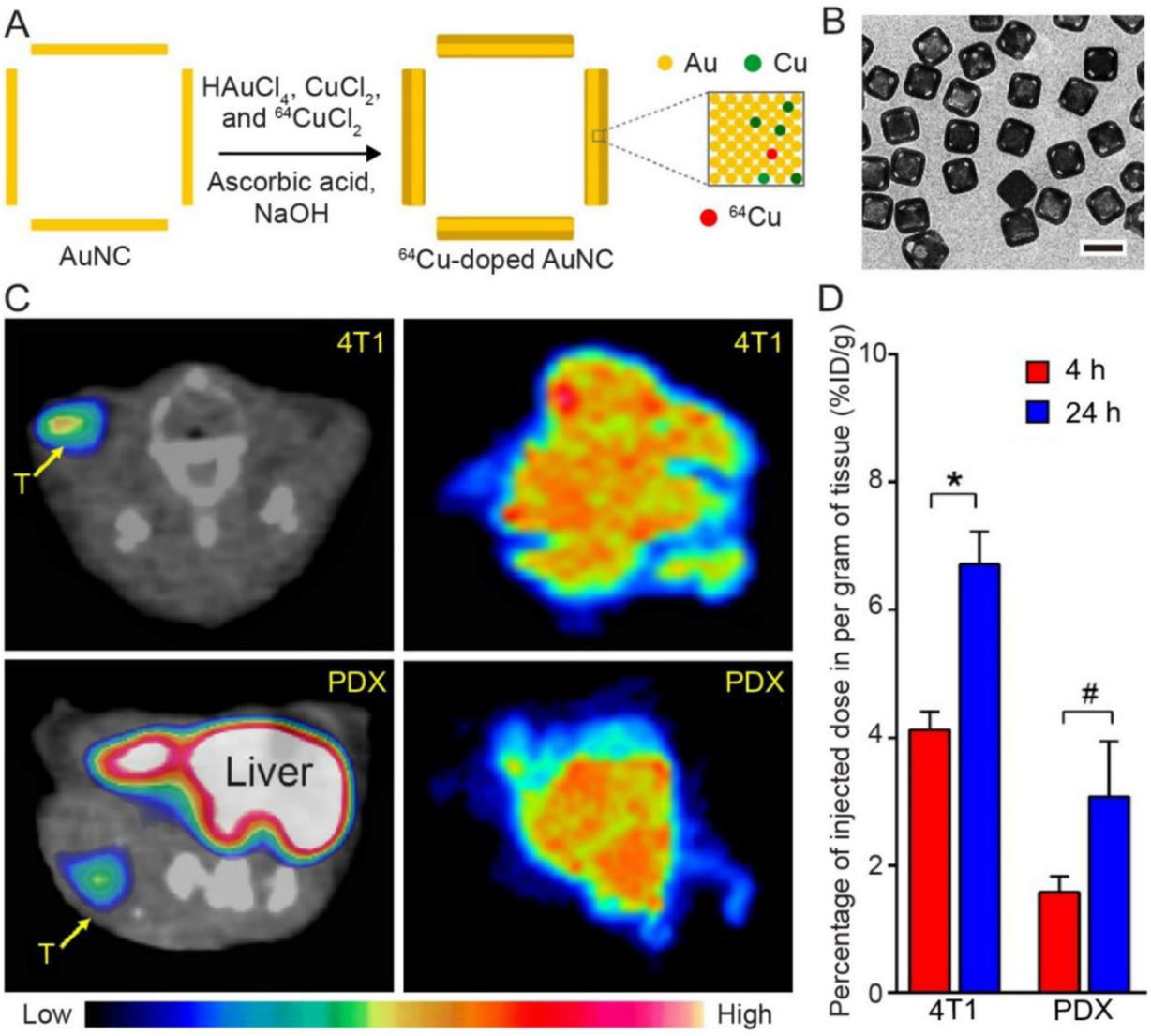

Figure 4.

(A) Schematic illustration showing the synthesis of a ^{64}Cu-doped AuNCs through co-deposition of Au, Cu, and ^{64}Cu atoms onto the walls of AuNCs. (B) TEM image of AuNCs after deposition of a layer of Au-Cu alloy (3.6 nm in thickness). (C) Transverse PET/CT images (left) and autoradiographs (right) of the PEGylated, ^{64}Cu-doped AuNCs in mice 4T1 and PDX tumor models at 24 h post injection. (D) Quantification of tumor uptake in both tumor models. *p<0.0005, #p<0.005. Reproduced with permission.[18] Copyright 2016, Wiley-VCH.

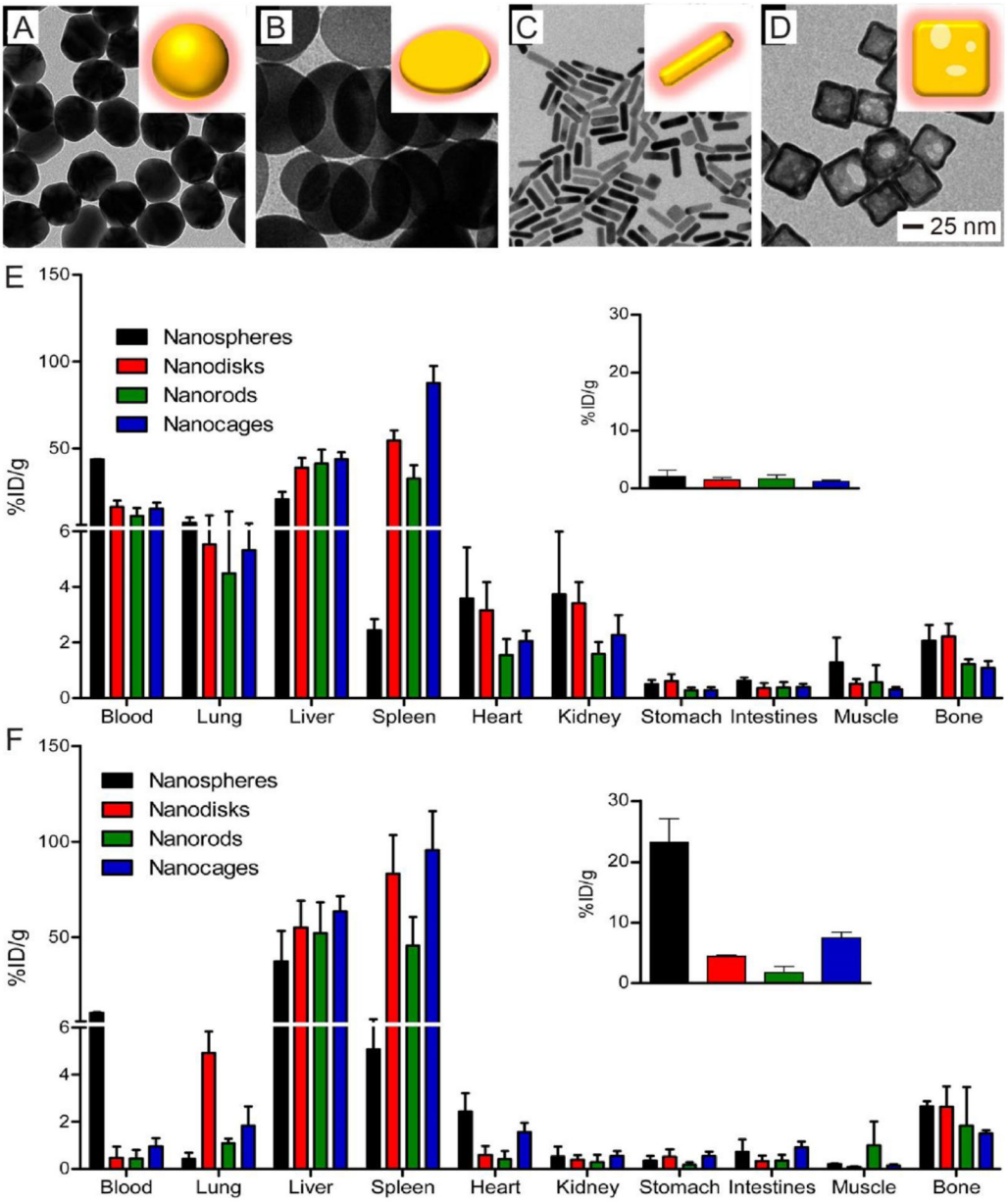

Figure 5.

(A–D) TEM images of Au-based (A) nanospheres, (B) nanodisks, (C) nanorods, and (D) nanocages, respectively. Quantitatively biodistribution of these four types of Au nanostructures, after labeling with ^{198}Au, at (E) 1 and (F) 24 h post injection. The insets in (E) and (F) show the tumor uptake data. Reproduced with permission.[49] Copyright 2014, American Chemical Society

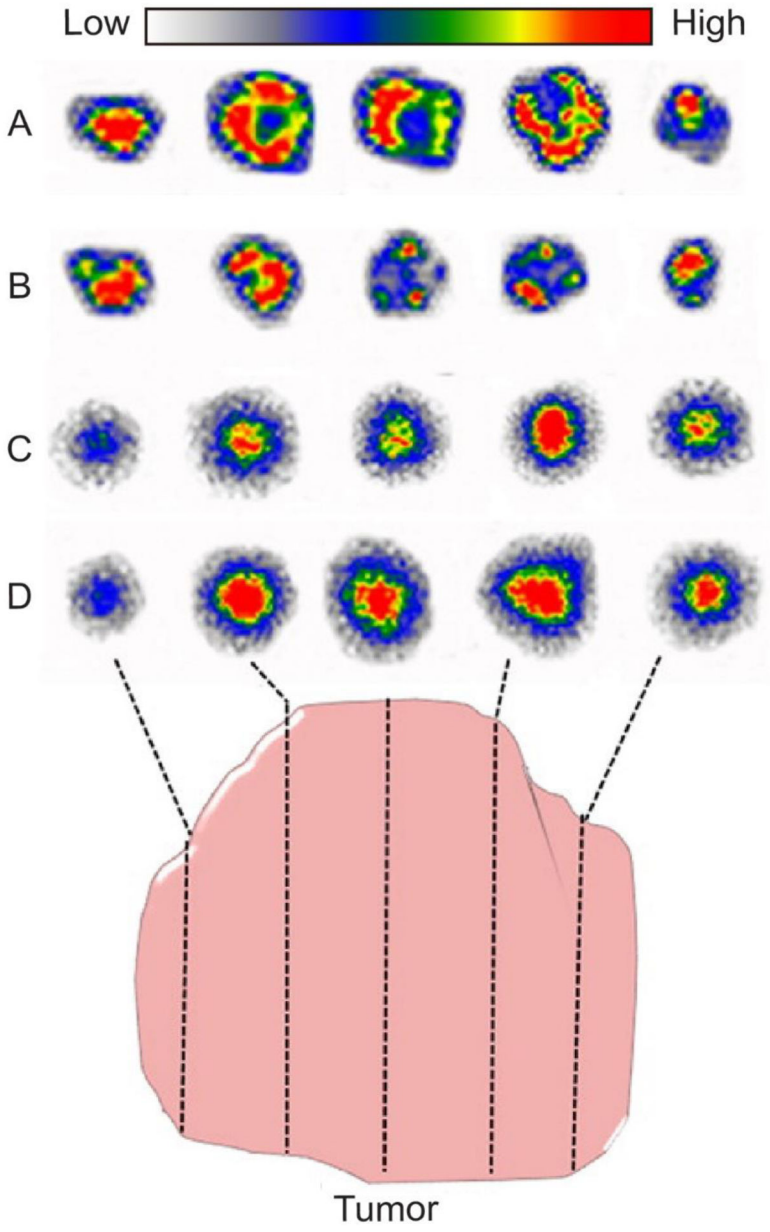

Figure 6.

Autoradiographic images of tumor slices at 24 h post injection of four types of ^{198}Au-labeled Au nanostructures: (A) nanospheres, (B) nanodisks, (C) nanorods, and (D) nanocages, respectively. Reproduced with permission.[49] Copyright 2014, American Chemical Society.

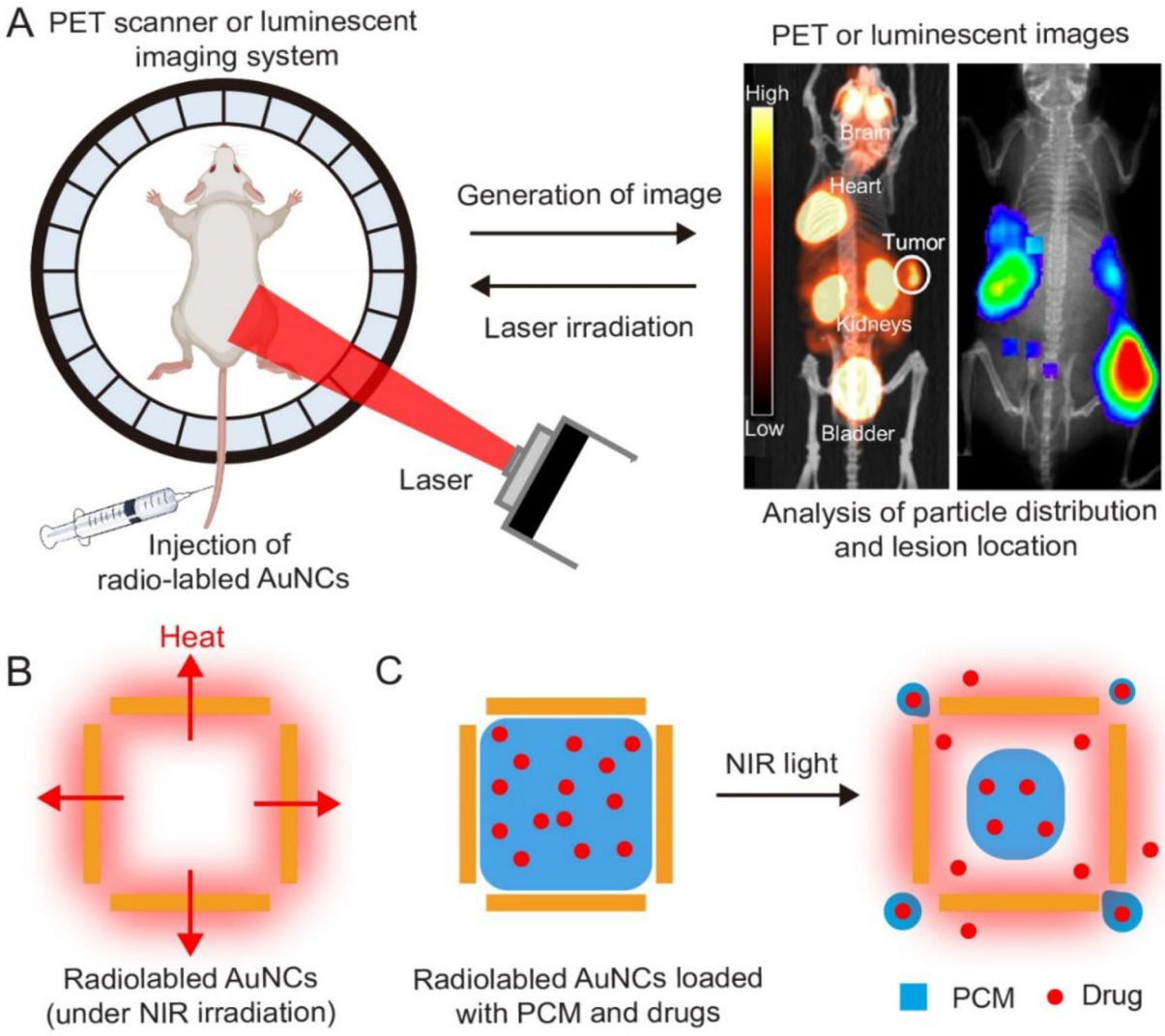

Figure 7.

(A) Schematic illustration showing the potential use of radiolabeled AuNCs in image-guided therapy. The PET or luminescent imaging system can help confirm the boundaries of lesion tissues and the biodistribution of nanocages. With such information, the NIR laser can be applied to the exact position with an appropriate duration and powder. Under laser irradiation, the AuNCs are able to photothermally eradicate cancer cells. In the meantime, drugs can be loaded into the nanocages with a thermo-responsive material to enable temperature-controlled release. (B, C) Schematic illustrations showing the NIR-enabled (B) photothermal capability and (C) controlled release of a AuNC. The PET and luminesce images in (A) were adapted with permission.[17,35] Copyright 2012 and 2013, American Chemical Society.